



Available online at www.sciencedirect.com

ScienceDirect



Journal of Magnesium and Alloys 9 (2021) 1906–1921

www.elsevier.com/locate/jma

Review

A review on electromagnetic shielding magnesium alloys

Lizi Liu^{a,b}, Xianhua Chen^{b,c,*}, Fusheng Pan^{b,c,*}

^aChongqing Light Alloy Materials and Processing Engineering Technology Research Center, Chongqing Three Gorges University, Chongqing, 404130, China

^bCollege of Materials Science and Engineering, Chongqing University, Chongqing 400045, China

^cNational Engineering Research Center for Magnesium Alloys, Chongqing University, Chongqing 400045, China

Received 8 October 2021; received in revised form 27 October 2021; accepted 31 October 2021

Available online 5 December 2021

Abstract

Electromagnetic waves generated by electronic equipment are widely present in all living and working spaces because of the rapid development of electronic products and frequent use of digital systems. Electromagnetic shielding is an effective method of protection against these waves. Therefore, the demand for materials with high electromagnetic shielding properties has remarkably increased. Magnesium (Mg) alloys, as potential electromagnetic shielding materials, have sparked great interest worldwide. This review highlights the effects of grain size, texture, alloying elements and second phase on the shielding properties of Mg alloys. Recent progress on the shielding properties of Mg-Zn, Mg-Al, Mg-RE and other new shielding Mg alloys is then summarised, and the successful design of Mg alloys with superior electromagnetic shielding properties, such as Mg-Zn-Y-Ce-Zr, Mg-Sn-Zn-Ca-Ce, Mg-Gd-Y-Zn-Zr and Mg-based composite materials, is described. Finally, this review provides insights into the future development and applications of Mg alloys with superior shielding properties.

© 2021 Chongqing University. Publishing services provided by Elsevier B.V. on behalf of KeAi Communications Co. Ltd.

This is an open access article under the CC BY-NC-ND license (<http://creativecommons.org/licenses/by-nc-nd/4.0/>)

Peer review under responsibility of Chongqing University

Keywords: Magnesium alloys; Electromagnetic shielding; Mechanical properties; Microstructure; Influencing factors.

1. Introduction

Electromagnetic shielding, which effectively protects electronic equipment from serious electromagnetic interference (EMI) and radiation, has recently sparked great interest [1–10], and the demand for materials with high EMI shielding capacity has drastically increased [11–13]. Metals and polymer composites are often used as EMI shielding materials. However, conventional metals with good EMI shielding capacity and superior mechanical properties, such as copper and nickel, are heavy [2,5,14]. The application of composite materials as EMI shields is limited by their mechanical flexibility and high cost [15–17]. Thus, the development of new materials with excellent shielding effectiveness (SE), low density and suitable mechanical properties is an urgent undertaking.

Mg and its alloys have gained wide research attention on account of their low density, high specific stiffness, high specific strength, excellent damping capacity and recyclability [18–23]. Mg alloys have been recently discovered to be potential electromagnetic shielding materials [24–28]. A sharp increase in the literature on Mg shielding properties can be observed in the Web of Science Core Collection database. Domestic and foreign research institutions, such as Chongqing University and National University of Singapore, have conducted numerous studies on EMI shielding Mg alloys. Mg alloys are characterised with lower weight compared with other shielding metals given the same thickness [29,30]. However, the applications of these alloys are limited because of their relatively lower strength, plasticity, and corrosion properties than their competitors, such as aluminum (Al) alloys [31–34]. Many effective approaches, such as alloying, have been carried out to enhance the properties of Mg alloys [35–38]. Unfortunately, when the mechanical properties of Mg alloys are improved, their SE of EMI usually decreases to different degrees because of various complex factors. SE and

* Corresponding author.

E-mail addresses: xhchen@cqu.edu.cn (X. Chen), fspan@cqu.edu.cn (F. Pan).

mechanical performance usually show opposite trends. For example, rolled Mg–9Li alloys have an excellent SE of 96–102 dB but a relatively low ultimate tensile strength (UTS) of <170 MPa, which is insufficient to meet the demands of high-end devices [25]. Thus, researchers have exerted considerable efforts to address this issue. Understanding the factors influencing the shielding properties of Mg alloys is necessary to achieve the best comprehensive performance. Therefore, in this review, we describe and summarize the effects of grain size, texture, alloying elements and second phase on the shielding properties of Mg alloys. Recent progress on the shielding properties of several representative Mg alloys, such as Mg–Zn, Mg–Al and Mg–RE series, are also reviewed in detail. The present review can help enhance the understanding of this scientific field and promote the development and application of Mg alloys with excellent shielding performance on a global scale.

2. Mechanisms of EMI shielding

Electronic equipment can be effectively protected from EMI by using shields and covers [39,40]. The shielding body is usually made of conductive or magnetic materials. EMI energy is reflected and limited to a certain range through the shielding body [41–43]. The SE (unit, dB) is used to quantify the shielding properties of materials. The transmission line analogy proposed by Schelkunoff is commonly used to measure the SE of EMI of various materials [44–48]. The total SE (SE_{tot}) can be expressed as:

$$SE_{tot} = SE_R + SE_A + SE_B \quad (1)$$

where SE_R , SE_A and SE_B are the reflection, absorption and multiple reflection losses, respectively. A large portion of the incident field is reflected and a small portion is transmitted by a good metal shield [49,50]. Therefore, metal shields usually have a large SE_R at the first air/shield interface. Absorption loss occurs when electromagnetic waves penetrate the shield. SE_R is defined as:

$$SE_R = 20\log_{10} \frac{|1+k|^2}{4|k|} \quad (2)$$

where k is the ratio of Z_s/Z_o , Z_o is the characteristic impedance of free space and Z_s is the intrinsic impedance of metal shield (in Ω). Z_o is usually a constant ($\sim 377 \Omega$). For low-Z match or high-Z mismatch shields, k is minimal, which results in a large SE_R . The magnitude of SE_R depends mainly on the relative mismatch between incoming waves and the surface Z of the shield [51–53]. SE_A can readily be expressed as [54,55]:

$$SE_A = 20\log_{10}(e^{t_s/\delta_s}) = 8.686 \left(\frac{t_s}{\delta_s} \right) \quad (3)$$

where δ_s is the skin depth (in m) and t_s is the shield thickness (in m). The multiple reflection correction term accounts for the reduction in SE under low absorption loss due to multiple reflections inside the shield [56–58]. This parameter is given

by:

$$SE_B = 20\log_{10} \left| 1 - \frac{(k-1)^2}{(k+1)^2} e^{-\frac{2t_s}{\delta_s}} \right| \quad (4)$$

The conductivity of pure Mg is 2.3×10^7 S/m, which is approximately 40% that of pure copper (Cu). Mg alloys with good conductivity have excellent electromagnetic shielding properties. The main electromagnetic shielding mechanism of most Mg alloys is SE_R . Mg alloys are non-magnetic materials with $\mu = 1$. Therefore, SE_R usually depends on the conductivity of Mg alloys. Excellent conductivity means a low Z_s/Z_o value, and leads to more electromagnetic waves reflected from the surface of Mg alloys consequently. With the detailed investigation of electromagnetic shielding Mg alloys, multiple reflections can be significantly improved by increasing the number of fine second phases and the density of grain boundaries, which provide discontinuous reflective interfaces. However, excessive amounts of concentrated second phases decrease the number of discontinuous reflective interfaces and reduce the electromagnetic shielding properties of an alloy. Additionally, new shielding Mg alloys containing micro-particulates are capable of multiple reflections. Adding micro-particulates to Mg alloys can form pores/holes, which enhances the production of multiple reflections. For example, the SE of pure Mg with 5 wt.% titanium (Ti) micro-particulates (72 dB) is higher than that of pure Mg [30]. In General, based on the mentioned theory of electromagnetic shielding of Mg alloys, various factors such as grain size, alloying elements, second phase and texture influence the shielding properties of Mg alloys.

3. Factors influencing EMI shielding properties of Mg alloys

3.1. Grain size

In recent years, many studies on the effect of grain size on the microstructure and mechanical properties of Mg alloys have been widely reported [59–63]. However, the investigation of the impact of grain size on EMI shielding Mg alloys is still limited. Recently, the effect of grain size on the SE of EMI of different Mg alloys has been studied [64, 65]. For instance, the values of SE of hot-rolled AZ31 alloys with varying grain sizes are fairly similar at low frequencies. Even at high frequencies, the maximum difference in SE at 1200 MHz is only 5 dB [64]. The effect of defects on the shielding properties of Mg alloys has also been investigated, and the grain size of alloys obtained using steel mold casts has been found to be three times greater than that of alloys obtained using Cu mold casts [65]. The increase in SE of EMI within the combined frequency range is only 4%.

The behavior of electron flow and its interaction with the grain boundaries has been studied [65]. Electron flow is obstructed by grain boundaries and then scattered, leading to weak vortex electrical currents and, in turn, low conductivity. Conductivity decreases with increasing electron scattering

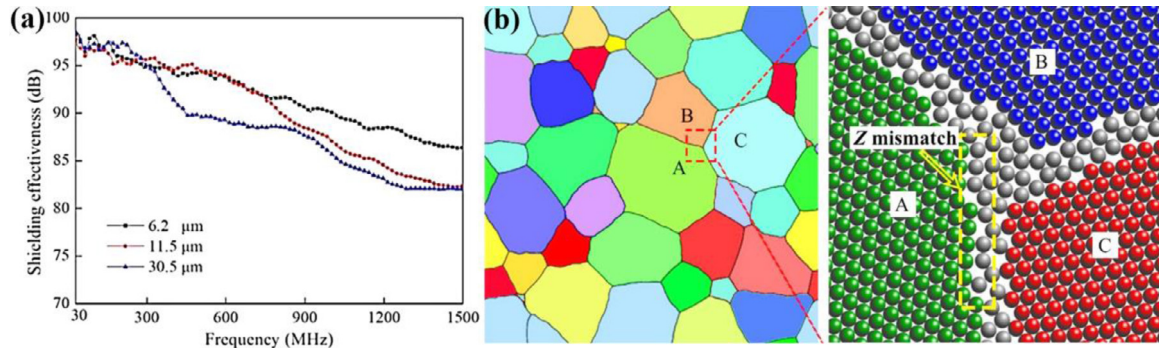


Fig. 1. (a) SE curves of 60%-AZ31 samples with different grain size. (b) The schematic drawing of impedance (Z) discontinuous (or mismatch) on grain boundary [64].

when the grain size is small, and poor conductivity may cause unsatisfactory SE [66]. When electromagnetic waves propagate in materials, they can be reflected and refracted when the interfaces feature different Z. A large Z mismatch results in high SE. Fig. 1(b) illustrates Z discontinuity (or mismatch) at the grain boundary. The grain boundary of Mg alloys is a very weak discontinuous interface, which leads to a low-Z mismatch between adjacent grains. Consequently, when the grain size changes, the SE of Mg alloys is only affected to a small extent [64]. In general, the contribution of grain size at the micron scale to the overall SE of Mg alloys may be considered negligible. When the grain size reaches the nanometre level, however, the conductivity of the material changes significantly [67], and the electromagnetic shielding performance of the alloys may be substantially affected by this phenomenon. Unfortunately, no report on the effect of grain size at the nano-scale on the shielding properties of Mg alloys is yet available.

3.2. Texture

Wrought Mg alloys usually show a strong texture, which significantly influences the properties of the alloys [68–71]. Recently, the effect of texture on the shielding properties of Mg alloys has been investigated. Unlike grain size, the impact of texture on the shielding properties of Mg alloys cannot be ignored [37]. Similar conclusions are made in Ref. [72]. It is suggested that the uniform grain orientation is beneficial to the development of EMI shielding Mg alloys with high SE. The influence of rolling strain on the electromagnetic shielding properties of dual-phase Mg–9Li alloys has been evaluated [24]. As the rolling strain increases, the c-axis direction of most grains changes from a random orientation to a normal direction (ND), as illustrated in Figs. 2(a)–(c). The basal texture intensity after rolling is much stronger than that before rolling, which means more grains acquire the same orientation. Compared with the un-rolled alloy, the SE of the alloy subjected to 80% rolled deformation increases by 6.17 and 9.59 dB at 200 MHz and 1.2 GHz, respectively. A large plane composed of grains with uniform orientation greatly contributes to the enhancement of the shielding properties of Mg alloys. Fig. 2(e) shows a schematic diagram of the grain

Table 1
EMI SE of as-solution Mg–1at.%X alloys in selected frequency [64].

Alloys	Content (at.%)	Conductivity (MS/m)	Shielding effectiveness (dB)		
			900 MHz	1200 MHz	1500 MHz
Mg–Zn	1.14	19.21	88	95	81
Mg–Al	1.10	16.11	80	80	80
Mg–Sn	1.07	10.26	74	70	63
Mg–Y	0.84	10.02	74	71	66
Mg–Gd	0.81	9.10	70	60	59

orientation of dual-phase structures. The increasing planes of grains composition in the α -Mg and β -Li phases can reflect electromagnetic waves very well.

Additionally, Song et al. described the effect of texture on the electromagnetic shielding properties of Mg alloys in detail [37]. As shown in Fig. 3, the texture intensity increases with increasing rolling reduction of the AZ31 sheets. The SE increases with the basal texture intensity, and the basal plane of most grains is parallel to the rolling surface. The reduction of the surface Z of the sheets increases the Z mismatch between the air and the alloy samples. According to electromagnetic shielding theory, a large Z mismatch leads to more incident electromagnetic wave reflection, which improves SE_R and SE_{tot} . In general, texture is one of the important factors affecting the EMI shielding properties of Mg alloys. The deformation process changes the texture and grain orientation of Mg alloys. Uniform grain orientation is beneficial to improve the electromagnetic shielding performance of Mg alloys.

3.3. Alloying elements

Alloying elements, such as Al, Sn, Y and Gd, are widely used to improve the mechanical properties of Mg alloys [73,74]. However, the presence of alloying elements in the solid-solution state in Mg alloys deteriorate their SE of EMI. Several comprehensive investigations of the effects of alloying elements on the shielding properties of Mg alloys have been reported [3,29]. The SE of binary Mg–Zn, Mg–Al, Mg–Sn, Mg–Y and Mg–Gd alloys bearing alloying elements existing in the solid-solution state have been discussed in detail [29,64]. As shown in Table 1, the effects of these alloying

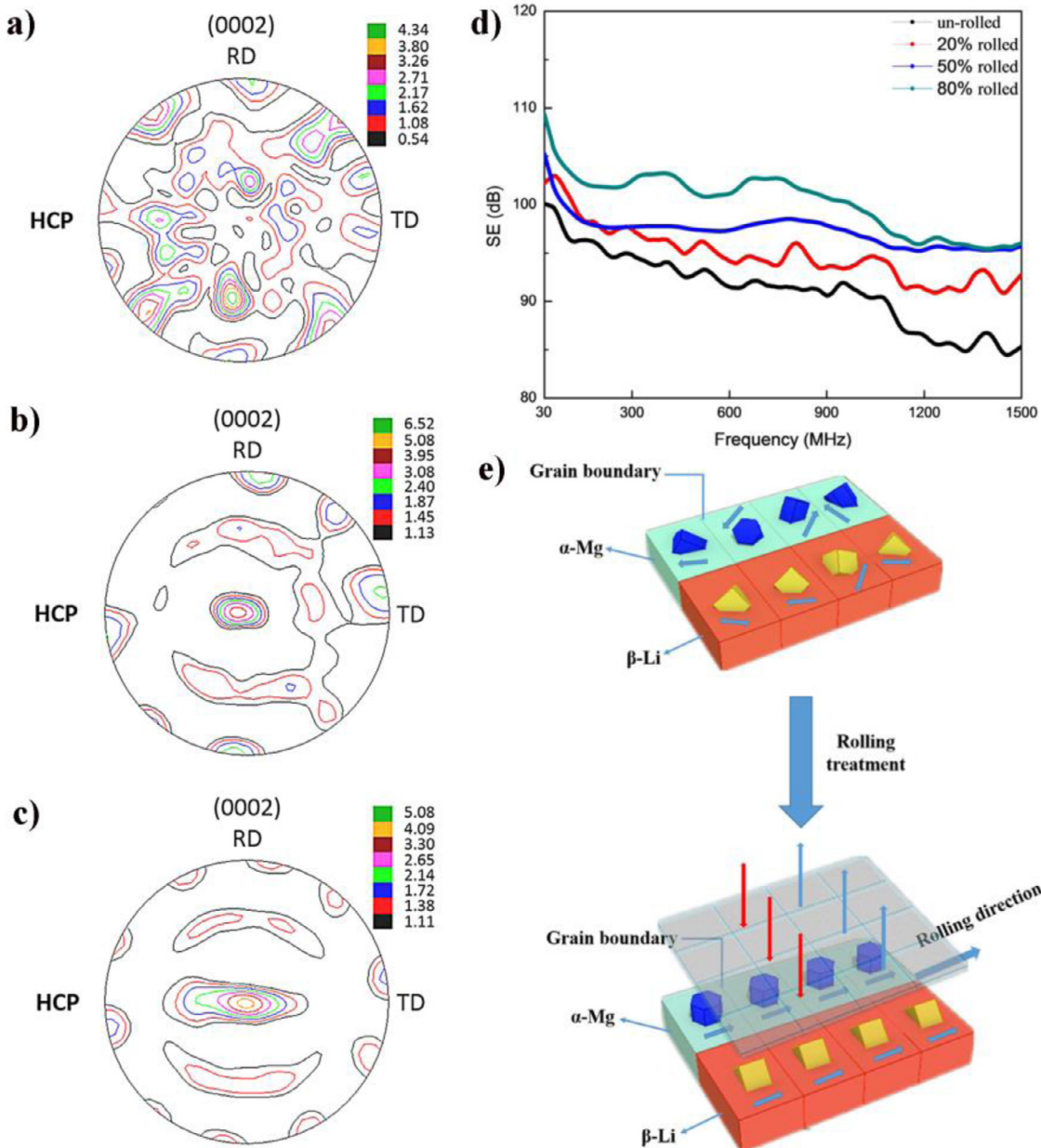


Fig. 2. Basal textural evolution of Mg–9Li alloy under different states: (a) un-rolled, (b) 20% rolled and (c) 80% rolled. (d) SE curves and (e) schematic diagram of grain orientation of the dual-phase structure [25].

elements on SE show the order Zn < Al < Sn < Y < Gd. The SE significantly decreases with increasing alloying elements additions because of the increase in the solid solution of alloying elements in α -Mg matrix. The effect of solute atoms on the SE of Mg alloys is generally governed by various factors, such as the volume difference rate between solute atoms and Mg atoms $\Delta V/V_{Mg}$ [75,76]. The larger the $\Delta V/V_{Mg}$, the more serious the distortion of the Mg lattice. Serious scattering during electron transmission leads to low conductivity [77,78], which, in turn, causes the Z_S of the alloy to decrease and weakens the SE_R [79–81]. Moreover, poor conductivity decreases the internal electromagnetic induction eddy current loss, which reduces the SE_A in some Mg alloys

[82–84]. Therefore, alloying elements with low solubility in the α -Mg matrix should be selected when designing Mg alloys with high SE. Another effective approach to improve the SE is to precipitate alloying elements from the supersaturated matrix into second phase.

3.4. Second phase

The effect of second phase on the shielding properties of Mg alloys is complicated. The number, size and orientation of second phase significantly affect the shielding properties of Mg alloys. Yang et al. found that SE could be enhanced by the addition of Sm to Mg–Zn–Sm–Zr alloys [85]. The

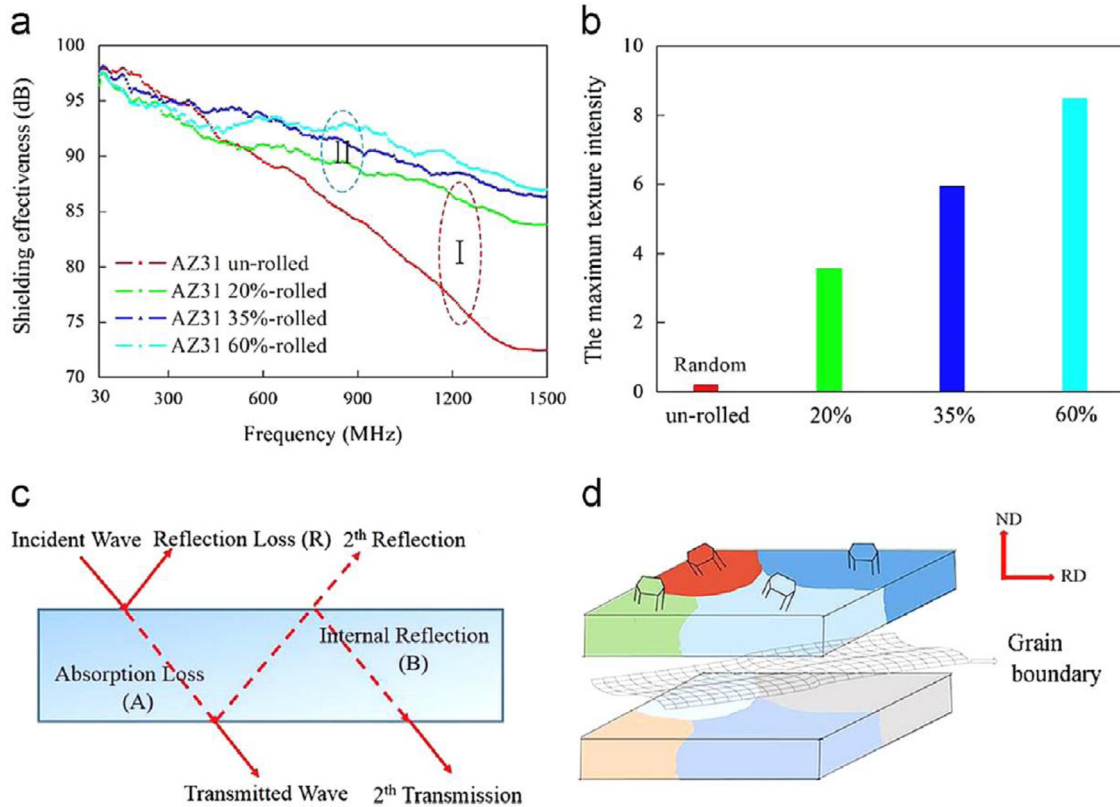


Fig. 3. (a) SE of investigated AZ31 specimens during 30 ~ 1500 MHz range; (b) the maximum texture intensity of un-rolled, 20% and 35%, 60% rolled AZ31 alloy samples; (c) mechanism of EMI shielding; and (d) schematic representation of the grain orientation and microstructure of the alloy [28].

precipitation of Sm-containing rare-earth (RE) phase consumes solid-soluted Zn atoms in α -Mg matrix, which leads to lattice distortion reverting. Thus, the SE raises with the increasing number of Sm-containing phases. Furthermore, the number of second phase interfaces also increases, which is beneficial for electromagnetic wave reflections. However, excessive addition of these alloying elements to Mg alloys greatly increases the probability of second phase coarsening, resulting in serious lattice distortion and a discontinuous interface between second phase and α -Mg matrix, which, in turn, hinders electron transmission and reduces the SE [86]. Additionally, coarse second phase can impede the formation of eddy current circuits more compared to fine precipitate. Blockage of electron transport reduces conductivity and results in poor electromagnetic shielding performance [81,87]. Investigations on this topic are reported in detail in Refs. [88–91]. Similarly, Zhang et al. has studied the SE and corrosion resistance of Mg alloys fabricated by electro-pulsing [92]. As shown in Fig. 4(b), the SE of the alloys (~87 dB) at a high frequency (1500 MHz) increases by 109.4%. The number and size of precipitates simultaneously decrease in different electro-pulsing treatments, as shown in Figs. 4(c) and (d). The enhanced SE is attributed to the dissolution and refinement of precipitates.

Up to now, it has been found that the orientation of second phase is one of the vital factors affecting the shielding proper-

ties of Mg alloys [93,94]. Chen et al. in Chongqing University systematically studied the effect of second phase orientation on the EMI shielding performance of Mg alloys [93]. A comparison of the effects of second phase with different orientations on the SE of Mg-Zn and Mg-Sn alloys is presented in Figs. 5(a) and (b). The SE is improved when precipitates form along the basal plane perpendicular to the incident direction of electromagnetic waves. The improvement in SE, however, is not as apparent when precipitates are oriented along other planes. The orientation of $MgZn_2$ and Mg_2Sn phases is different, as illustrated in Fig. 5(c). Plate-like Mg_2Sn phases form an infinite plate along the basal plane, thereby forming a theoretical model similar to that in Fig. 5(d). Electromagnetic waves are reflected when they pass through the plate-shaped Mg_2Sn phase vertically. Ultimately, the SE_R and SE_B of incident electromagnetic waves are significantly enhanced.

The discussion above clearly reveals that the number, size, shape and orientation of second phase affect EMI shielding Mg alloys. Therefore, further investigation of approaches to control these factors to obtain high-performance Mg alloys is necessary.

Based on the influencing factors of EMI shielding Mg alloys, various Mg alloys with superior EMI shielding properties have been developed. At present many studies focus on Mg-Zn, Mg-Al, Mg-RE and other new EMI shielding Mg alloys. In the following subsections, we summarize the

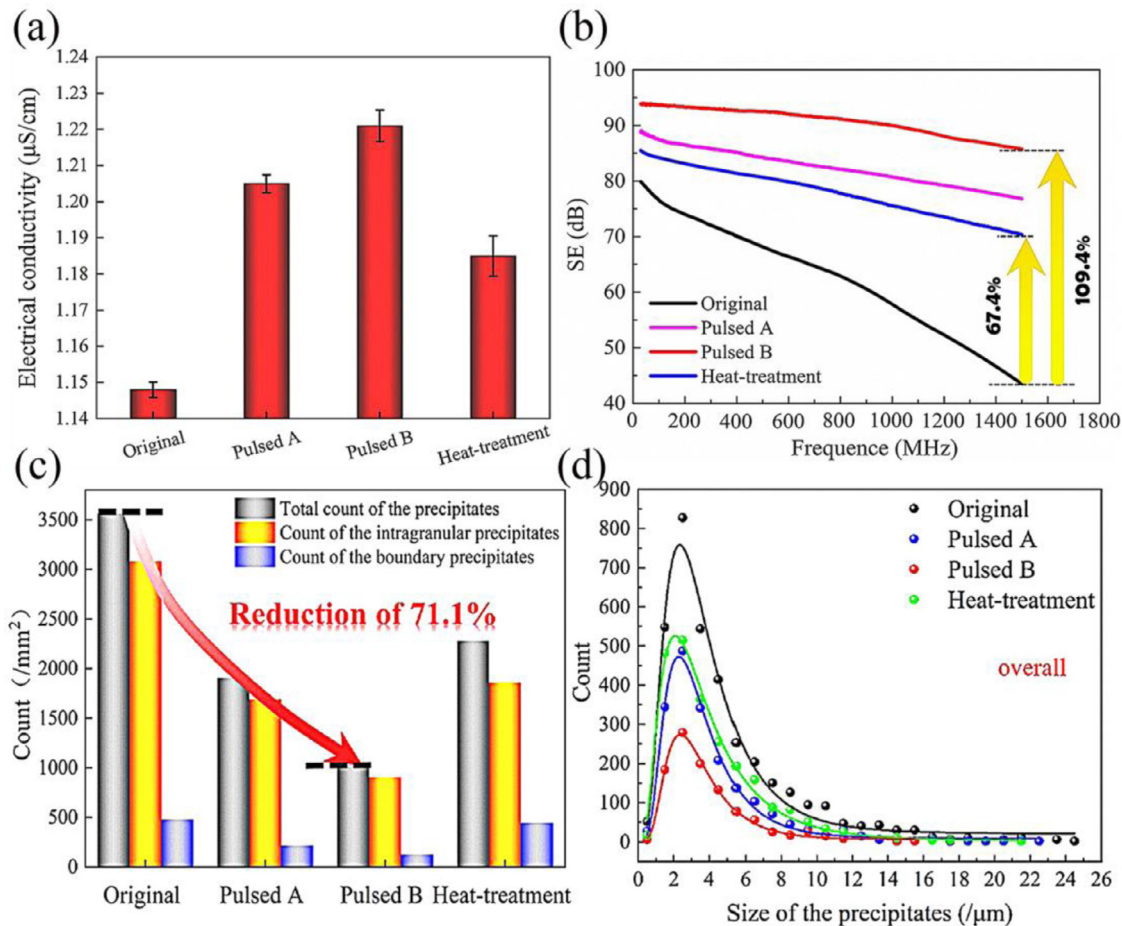


Fig. 4. (a) and (b) Electrical conductivity and SE of Mg alloys in different treatment state. Statistical results of (c) the total number of precipitates at different positions and (d) the overall size distribution of precipitates, respectively [92].

EMI shielding properties of these alloys based on recent references.

4. Electromagnetic shielding Mg alloys

4.1. Mg-Zn series alloys

Zn is one of the most momentous alloying elements in commercial Mg alloys such as ZK, ZM, ZW, and ZE series alloys [95,96]. Mg-Zn binary alloys exhibit favorable SE but poor mechanical properties due to their coarse grains. Thus, addition of alloying elements is necessary to refine the microstructure of the alloys and balance their shielding performance and mechanical properties. Suitable alloying elements include some RE-free elements, such as Zr, Cu and Mn, and RE elements. EMI shielding Mg-Zn-Zr, Mg-Zn-Cu, Mg-Zn-RE alloys have been successfully developed. Table 2 lists the SE and mechanical properties of various Mg-Zn series alloys. These alloys, especially Mg-Zn-RE alloys with various RE element additions, have excellent electromagnetic shielding performance and good mechanical properties.

Mg-Zn-Zr and Mg-Zn-Cu alloys are typical RE-free shielding Mg-Zn series alloys. Zr can significantly refine the

grains of binary Mg-Zn alloys [97,98] and combine with Zn to form the ZnZr phase, thereby increasing the reflection interface of electromagnetic waves. In the case of as-cast Mg-3Zn-0.5Zr alloy, the SE of 75 dB at 1500 MHz was achieved [85]. The solid solubility of Zn in α -Mg matrix decreases by heat treatment or addition of alloying elements, which weakens lattice distortion and improves SE. Liu et al. obtained an aged Mg-6Zn-0.5Zr alloy and found that this material has an SE of over 70 dB and good mechanical properties, as shown in Table 2 [88]. If cold-rolling is performed prior to artificial aging, more nucleation is provided during precipitation, and the aging process is promoted to obtain higher SE and improved mechanical properties [99]. The SE and yield strength of cold-rolled and aged Mg-6Zn-0.5Zr is as high as 71 dB (1500 MHz) and 311 MPa, respectively. Addition of RE-free elements, such as Cu, could reduce the cost of EMI shielding Mg alloys. The conductivity of Cu is superior to those of all commonly used structural metals [100,101]. Cu addition can increase the eutectic temperature, and so a higher solution treatment temperature for Mg-Zn series is available [102,103]. Cu is combined with Zn to form the MgZnCu phase, which leads to reductions in the solid solubility of Zn in α -Mg matrix. Therefore, Mg-Zn-Cu-Zr alloys demonstrate excellent electromagnetic shielding properties, as shown

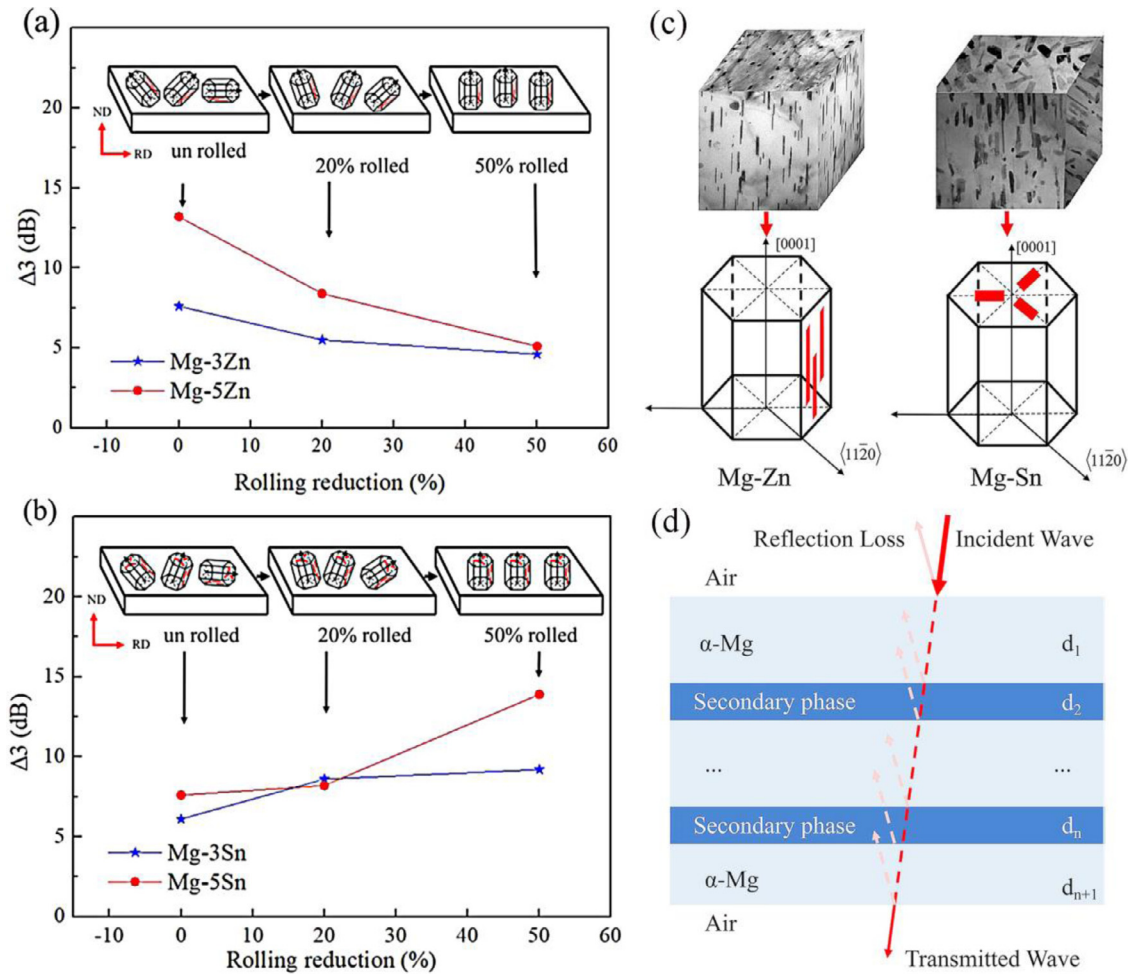


Fig. 5. Effect of second phase orientation on the electromagnetic shielding properties of (a) Mg-Zn and (b) Mg-Sn alloys ($\Delta 3 = SE_{aged} (60 \text{ h}) - SE_{solutionized}$), respectively. (c) Schematic of second phase orientation. (d) Double-layer shield model [93].

in Table 2 [90]. Mg-5Zn-2.5Cu-0.6Zr shows optimal EMI shielding capacity with an SE of 84 dB at 1500 MHz. However, the mechanical properties of this alloy are poor because of the coarse MgZnCu phase.

Generally, Mg-Zn alloys containing RE exhibit reliable mechanical properties and creep resistance at elevated temperatures due to grain refinement, RE-containing phase and texture weakening effects [104,105]. These RE elements mainly include Y, Ce, Gd and Sm. The effects of Y, Ce and the combination of Y and Ce on the SE and mechanical properties were studied by Chen et al. [89,106,107]. The SE is remarkably improved by Y or Ce addition. Thus, enhanced shielding effects are expected when various RE elements are added to the alloy. Superior SE and mechanical properties are obtained when Y and Ce are simultaneously added to Mg-Zn-Zr alloy, as shown in Figs. 6(a) and (b). The SE of the extruded Mg-5Zn-1Ce-2Y-0.5Zr alloys reached 79–118 dB over the whole frequency range tested [108]. Moreover, a high yield strength of over 400 MPa, which is significantly higher than that of commercial Mg-Zn-Zr alloys, is successfully obtained for this alloy [31]. The stable RE-containing phase and fine precipitates shown in Figs. 6(c)–(h) provide

considerable contributions to the improvement in the SE and strength.

Many types of Mg-Zn-RE phases could be formed depending on the type of RE element added. The different phases formed have multiple effects on the SE and mechanical properties of the alloys. The SE (73 dB at 1500 MHz) of Mg-2Zn-4Y with long period stacking ordered (LPSO) phases is higher than that of some previously studied alloys [24]. However, research on the effect of the LPSO phase on electromagnetic shielding remains relatively rare. Xu et al. studied the effect of the LPSO phase on the electromagnetic shielding performance of directionally solidified Mg_{98.5}Zn_{0.5}Y₁ alloys, as shown in Fig. 7 [94]. The SE of the alloy with dispersed lamellar LPSO phase is ~15 dB higher than that of alloy with randomly distributed LPSO phase. The higher the orientational consistency of the LPSO phase precipitated in a specific direction, the higher the SE_R .

4.2. Mg-Al series alloys

Mg-Al series alloys are widely used in the engineering field [109–111]. The main strengthening phase of these al-

Table 2

Electrical conductivity, SE and mechanical properties of Mg-Zn series alloys.

Materials	Processing conditions	SE/dB	SE/dB	Mechanical properties			Ref.
		(f = 900 MHz)	(f = 1500 MHz)	UTS (MPa)	YS (MPa)	EL (%)	
Mg-5Zn-0.6Zr	Extruded	85	66	318	246	9.7	[90]
Mg-5Zn-1Zr	Extruded	83	65	318	231	11	[89]
Mg-6Zn-0.5Zr	Extruded	58	54	302	231	11	[106]
Mg-3Zn-0.5Zr	As-cast	83	75	—	—	—	[85]
Mg-6Zn-0.5Zr	150 °C × 4 h aged	66	64	303	241	20	[88]
	150 °C × 15 h aged	72	70	316	269	20	[88]
	150 °C × 50 h aged	75	65	313	285	19	[88]
	cold rolled + 150 °C × 15 h aged	75	71	368	311	7	[99]
	cold rolled + 150 °C × 50 h aged	76	81	355	302	10	[99]
	T4 (400 °C, 5 h)	55	53	315	232	25	[56]
	T4 (400 °C, 5 h) + T5 (130 °C, 4 h)	59	54	319	252	20	[56]
	T4 (400 °C, 5 h) + T5 (130 °C, 20 h)	61	57	319	252	20	[56]
	T4 (400 °C, 5 h) + T5 (170 °C, 25 h)	65	62	327	294	21	[56]
Mg-5Zn-0.5Cu-0.6Zr	Extruded	91	66	346	276	11.4	[90]
Mg-5Zn-1Cu-0.6Zr	Extruded	97	77	332	263	7.8	[90]
Mg-5Zn-1.5Cu-0.6Zr	Extruded	99	77	311	258	8.0	[90]
Mg-5Zn-2.5Cu-0.6Zr	Extruded	103	84	306	246	6.7	[90]
Mg-3Zn-1Y	As-cast	80	67	—	—	—	[24]
Mg-3Zn-3Y	As-cast	76	70	—	—	—	[24]
Mg-2Zn-4Y	As-cast	77	73	—	—	—	[24]
Mg-4Zn-8Y	As-cast	66	60	—	—	—	[24]
Mg-0.5Zn-1Y (at.%)	Directional solidification	87	71	160	60	3.8	[94]
Mg-0.5Zn-1Y-0.2Zr (at.%)	Directional solidification	~88	~70	270	120	~20	[94]
Mg-0.5Zn-1Y (at.%)	Directional solidification + asynchronous rolling	~93	88	230	80	—	[94]
Mg-5Zn-0.5Y-1Zr	Extruded	83	66	334	258	12	[89]
Mg-5Zn-1Y-1Zr	Extruded	89	76	321	265	8	[89]
Mg-5Zn-2Y-1Zr	Extruded	96	79	270	176	7	[89]
Mg-6Zn-0.5Ce-0.5Zr	Extruded	63	53	324	242	14	[106]
Mg-6Zn-1Ce-0.5Zr	Extruded	72	71	316	249	15	[106]
Mg-6Zn-2Ce-0.5Zr	Extruded	67	61	304	239	11	[106]
Mg-5Zn-0.5Y-1Ce-0.5Zr	Extruded	81	70	356	313	12.1	[107]
Mg-5Zn-1Y-1Ce-0.5Zr	Extruded	94	76	341	304	11.2	[107]
Mg-5Zn-2Y-1Ce-0.5Zr	Extruded	94	79	333	305	10.6	[107]
Mg-6Zn-0.2Y-0.5Ce-0.4Zr	Extruded	86	67	378	322	8.6	[108]
Mg-6Zn-0.5Y-0.5Ce-0.4Zr	Extruded	88	75	369	327	7.3	[108]
Mg-6Zn-1Y-0.5Ce-0.4Zr	Extruded	91	85	362	315	8.7	[108]
Mg-6Zn-1.5Y-0.5Ce-0.4Zr	Extruded	93	86	345	298	4.2	[108]
Mg-3Zn-1Sm-0.5Zr	As-cast	86	81	—	—	—	[85]
Mg-3Zn-2Sm-0.5Zr	As-cast	96	80	—	—	—	[85]

loys is $\text{Mg}_{17}\text{Al}_{12}$, which has a low melting point and, therefore, results in undesirable or unstable performance at room or high temperatures [112,113]. Zn, Mn, Sn and other RE elements are often added to these alloys to address this issue and improve their properties [114,115]. These alloying elements form high-melting point phase and reduce the $\text{Mg}_{17}\text{Al}_{12}$ phase simultaneously. Now many researchers have sought to improve the shielding and mechanical properties of Mg-Al series alloys synergistically [64,116–122]. Table 3 lists the SE and mechanical properties of Mg-Al series alloys. Song investigated the effect of Al and Zn on the electromagnetic shielding performance of as-cast Mg-Al-Zn alloys and found changes in SE as the proportions of Al and Zn varied, as indicated in Table 3 [64]. Generally, plastic deformation and heat treatment are conducted to improve the electromagnetic shielding and mechanical properties of Mg-Al series alloys. Zhang studied the effect of hot rolling and aging on the SE

of Mg-Al-Zn alloys and found that extruded Mg-6Al-1 Zn subjected to hot rolling at 325 °C shows a high SE of 87 dB at 1500 MHz and yield strength of 267 MPa [116]. The electromagnetic shielding and mechanical properties of this alloy are significantly improved compared with those of Mg-Al alloys. This finding may be attributed to the increase in SE_R caused by uniform grain orientation and the increase in internal SE_B caused by second phase and grain interfaces. RE element addition can effectively improve the electromagnetic shielding and mechanical properties of Mg-Al series alloys. La addition can gradually replace the original $\text{Mg}_{17}\text{Al}_{12}$ phase and preferentially form the new RE phase $\text{Al}_{11}\text{La}_3$. The SE of Mg-3Al-1Zn-0.35Mn-xLa ($x = 0.3\text{--}1.5$ wt.%) increases by 10 dB at 900 MHz as the La content increases from 0.3 wt.% to 1.2 wt.% [119]. The SE and mechanical properties as-cast Mg-7Al-1Zn-0.3Mn alloys initially increase and then decrease with increasing Y and Ce contents [118]. When Y

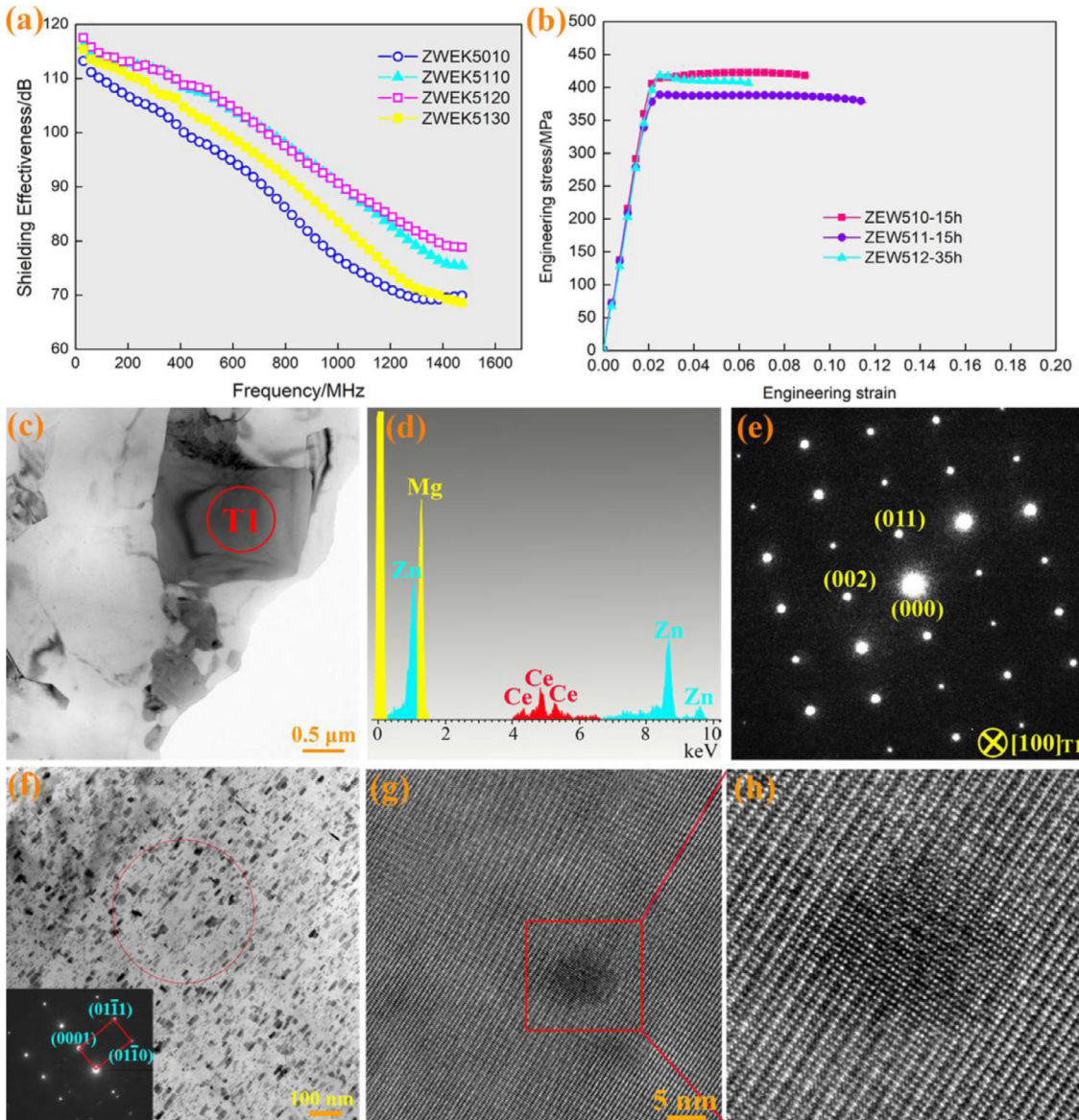


Fig. 6. (a) SE curves and (b) engineering stress-strain curves of extruded and aged Mg–Zn–Ce–Y–Zr alloys. TEM analysis of Mg–Zn–Ce (T1) structure in extruded Mg–Zn–Ce–Y–Zr bar: (c) morphology of Mg–Zn–Ce phase, (d) EDX analysis of Mg–Zn–Ce in (c), (e) SAED of red circle in (c), (f) fine precipitates, (g) and (h) HRTEM image of fine precipitates (MgZn_2) [108].

and Ce are simultaneously added to Mg–7Al–1Zn–0.3Mn alloy, the SE at 1500 MHz is 87 dB and its yield strength is 170 MPa. Mg–Zn series alloys with multiple RE element additions also show a similar trend for SE.

4.3. Mg–RE series alloys

The appropriate amount of RE elements can efficiently improve various properties and enhance the SE of Mg alloys at room and high temperature via the formation of RE-containing strengthening phases during appropriate heat treatment [123–129]. Gd, Y and Nd are usually selected to enhance the shielding and mechanical properties of these alloys synergistically. The SE and mechanical properties of most Mg–RE series alloys are summarised in Table 4. Mg–Gd series alloys bearing large amounts of Gd exhibit excellent

shielding and mechanical properties. For instance, the extruded and aged Mg–13Gd–4Y–2Zn–0.5Zr alloy show a superior SE of 96 dB at 1500 MHz and a high UTS of 381 MPa. Enhancements in the SE and mechanical properties of these alloys are associated with the formation of dispersed RE-containing precipitates, such as $\text{Mg}_5(\text{GdY})$, after aging [127]. In addition, Mg–Gd–Zn and Mg–Gd–Cu alloys with minor Gd addition also possess good SE [129]. Unfortunately, the high contents of heavy RE (e.g. Gd, Er, Yb) lead to inhomogeneous compositions and high costs. Therefore, efforts to develop EMI shielding Mg alloys with low RE element addition are well underway. A small amount of Nd addition to Mg alloys can strengthen the properties at room and high temperatures [71,114]. Mg–Y–Zr alloy with 2.63 wt.% Nd shows a good combination of mechanical properties and EMI

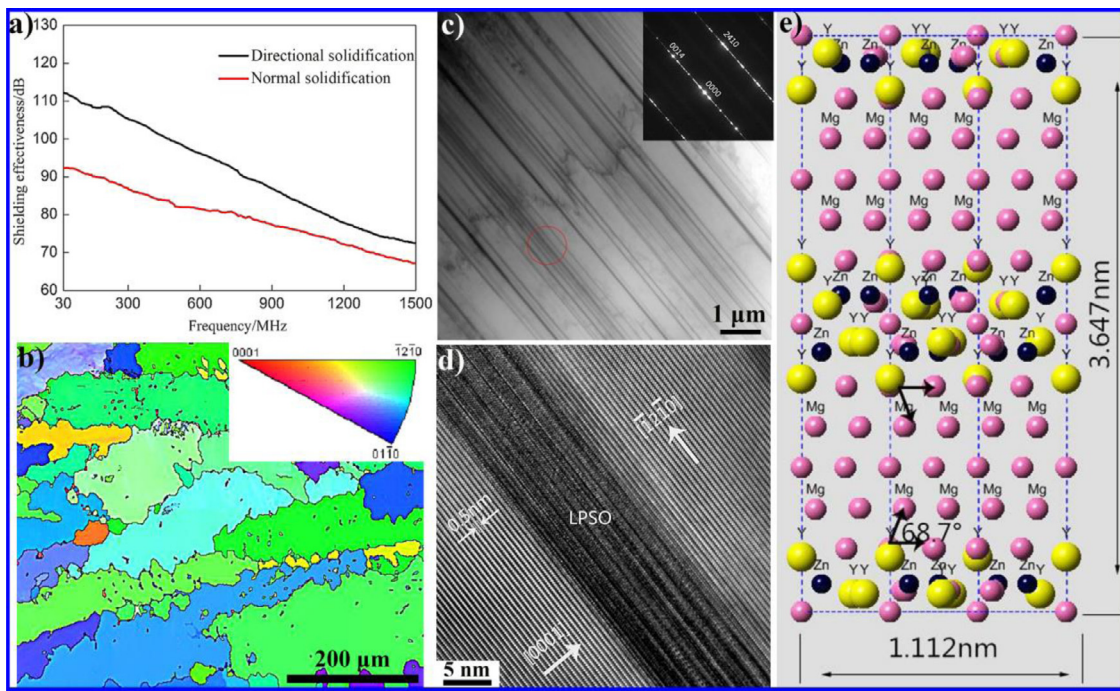


Fig. 7. (a) SE curves of $\text{Mg}_{98.5}\text{Zn}_{0.5}\text{Y}_1$ by normal and directional solidification. Microstructure analysis of $\text{Mg}_{98.5}\text{Zn}_{0.5}\text{Y}_1$ by directional solidification (b) IPF image, (c) TEM bright-field image, (d) HRTEM image and (e) an atomic model showing 14H-LPSO [94].

Table 3
Electrical conductivity, SE and mechanical properties of Mg-Al series alloys.

Materials	Processing conditions	SE/dB	SE/dB	Mechanical properties			Ref.
		($f = 900$ MHz)	($f = 1500$ MHz)	UTS (MPa)	YS (MPa)	EL (%)	
Mg-4Al-3Zn	As-cast	86	77	—	—	—	[64]
Mg-5Al-3Zn	As-cast	81	71	—	—	—	[64]
Mg-5Al-4Zn	As-cast	73	67	—	—	—	[64]
Mg-5Al-5Zn	As-cast	78	74	—	—	—	[64]
Mg-3Al-1 Zn	Hot rolled + annealed (450°C , 15 min)	80	74	262	172	13.9	[116]
Mg-6Al-1Zn	Extruded + hot rolled at 325°C	91	87	394	267	14.8	[116]
	T5 (200°C , 100 h)	76	72	330	177	13.6	[116]
Mg-8Al-1Zn-0.2Ti	T4 (440°C , 10 h)+T5 (220°C , 12 h)	75	62	—	—	—	[117]
	T4 (430°C , 10 h)+T5 (240°C , 12 h)	75	60	—	—	—	[117]
Mg-7Al-1Zn-0.3Mn-0.6Y	As-cast	~103	~77	~182	~143	~7.9	[118]
Mg-7Al-1Zn-0.3Mn-0.9Y	As-cast	~104	~88	195	157	8.9	[118]
Mg-7Al-1Zn-0.3Mn-0.9Ce	As-cast	~104	~81	187	147	9.6	[118]
Mg-7Al-1Zn-0.3Mn-1.2Ce	As-cast	~97	~81	~179	~144	~9.5	[118]
Mg-7Al-1Zn-0.3Mn-0.9Y-0.3Ce	As-cast	~91	~72	~202	~162	~9.0	[118]
Mg-7Al-1Zn-0.3Mn-0.9Y-0.9Ce	As-cast	~103	~87	~216	~170	~10.1	[118]
Mg-3Al-1Zn-0.35Mn-0.6La	T4 (410°C , 24 h) + T5 (200°C , 8 h)	~85	83	—	—	—	[119]
Mg-3Al-1Zn-0.35Mn-0.9La	T4 (410°C , 24 h) + T5 (200°C , 8 h)	~87	84	—	—	—	[119]
Mg-3Al-1Zn-0.35Mn-1.2La	T4 (410°C , 24 h) + T5 (200°C , 8 h)	~86	83	—	—	—	[119]
Mg-3Al-1Zn-0.35Mn-1.5La	T4 (410°C , 24 h) + T5 (200°C , 8 h)	~84	82	—	—	—	[119]
Mg-5.5Al-2.5Sn-0.1V	Extruded	79	72	—	—	—	[120]
Mg-6Al-2Sn-0.05Y	extruded at 260°C	~63	47	—	—	—	[121]
Mg-6Al-2Sn-0.05Y	extruded at 320°C	~71	65	—	—	—	[121]
Mg-6Al-2Sn-0.05Y	extruded at 380°C	~70	58	—	—	—	[121]
Mg-4Al-2Sn-0.1Y	As-cast	73	72	—	—	—	[122]

Table 4

Electrical conductivity, SE and mechanical properties of Mg-RE series alloys.

Materials	Processing conditions	SE/dB	SE/dB	Mechanical properties			Ref.
		($f = 900$ MHz)	($f = 1500$ MHz)	UTS (MPa)	YS (MPa)	EL (%)	
Mg-4Y-0.6Zr	Extruded	95	81	231	153	29.1	[91]
Mg-4Y-1Nd-0.6Zr	Extruded	84	71	274	216	24.2	[91]
Mg-4Y-4Nd-0.6Zr	Extruded	90	68	266	214	6.25	[91]
Mg-4Y-4Nd-0.6Zr	Extruded + T4 (525 °C, 8 h) + T5 (210 °C, 20 h)	81	63	322	177	7.19	[91]
Mg-4Y-3Nd-0.6Zr	Extruded + T4 (525 °C, 8 h) + T5 (210 °C, 40 h)	79	59	305	178	6.37	[91]
Mg-4Y-3Nd-0.6Zr	As cast + T4 (525 °C, 8 h)	85	77	—	—	—	[91]
Mg-4Y-3Nd-0.6Zr	As cast + T4 (525 °C, 8 h) + T5 (150 °C, 24 h)	97	87	—	—	—	[91]
Mg-13Gd-4Y-2Zn-0.5Zr	As cast	89	80	—	—	—	[127]
Mg-13Gd-4Y-2Zn-0.5Zr	Extruded in 45% deformation	101	89	298	224	5.9	[127]
Mg-13Gd-4Y-2Zn-0.5Zr	Extruded in 60% deformation	101	91	347	276	12.4	[127]
Mg-13Gd-4Y-2Zn-0.5Zr	Extruded in 80% deformation	102	93	380	310	10.8	[127]
Mg-13Gd-4Y-2Zn-0.5Zr	Extruded + T5 (225 °C, 24 h)	99	96	381	289	10.1	[127]
Mg-13Gd-4Y-2Zn-0.5Zr	Extruded + T5 (225 °C, 48 h)	99	94	347	291	8.1	[127]
Mg-13Gd-4Y-2Zn-0.5Zr	Hot upsetting at 460 °C	96	84	324	253	6.7	[128]
Mg-13Gd-4Y-2Zn-0.5Zr	Hot upsetting at 500 °C	93	83	319	248	6.8	[128]
Mg-13Gd-4Y-2Zn-0.5Zr	Hot upsetting at 460 °C + T5 (225 °C, 48 h)	100	89	343	274	5.0	[128]
Mg-5Gd-2Zn	As cast	~100	~80	99	68	3.5	[129]
Mg-5Gd-3Zn	As cast	~101	~93	85	62	2.1	[129]
Mg-5Gd-1Cu	Hot rolled	97	75	~250	~140	~12.5	[129]
Mg-5Gd-1Cu	As cast	~91	~70	140	117	4.4	[129]
Mg-5Gd-2Cu	Hot rolled	~93	~85	—	—	—	[129]
Mg-5Gd-2Cu	As cast	~95	~70	128	103	3.1	[129]

SE, as indicated in Table 4 [91]. Heat treatment significantly improves the SE of the alloy via the precipitation of the Mg-Y-Nd phase. The SE of as-cast Mg-4Y-3Nd-0.6Zr alloy increases to 87–106 dB when treated under the conditions of T4 (525 °C, 8 h) and T5 (150 °C, 24 h). Generally, achieving optimal balance between the shielding capacity and mechanical properties of EMI shielding Mg-RE alloys under low RE contents needs be further investigated.

4.5. Other shielding Mg alloys

Current research on the electromagnetic shielding performance of Mg alloys has become increasingly extensive and in depth. Some new shielding Mg alloy materials, such as RE-free Mg-Li series alloys, low-RE content Mg-Sn series alloys and shielding Mg-based composite materials, have been successfully developed [26,130,131]. Mg-Li series alloys with super-light characteristics have been fabricated by chemical composition design, heat treatment and plastic deformation to meet the requirements of more comprehensive applications [25,132]. Mg-9Li alloy exhibits excellent SE due to the numerous interfaces produced by duplex phases [26]. Wu et al. studied EMI shielding in a duplex-phase Mg-9Li-3Al-1 Zn alloy processed by accumulative roll bonding (ARB) [132]. Fig. 8 illustrates the corresponding three-dimensional optical micrographs and multi-layer interfacial electromagnetic shielding mechanism of duplex-phase Mg-9Li alloy. The SE of Mg-9Li-3Al-1 Zn alloy by ARB3 reaches 99 dB at 1200 MHz, as indicated in Table 5. Moderate mechanical properties are also obtained. As the ARB pass increases, the grain orientation of each layer tends to align along the

c-axis, which is beneficial to the SE_R and SE_B of incident electromagnetic waves. Low-cost Mg-Sn-Zn alloys also exhibit superior SE and high strength with Sn addition. The SE and strength of Mg-Sn-Zn-Ca-Ce alloys with minor amounts of Ca and Ce was studied [133,134]. The SE of such alloys is highest when the Sn content is 3 wt.%, as shown in Fig. 9(d). The SE of 91–114 dB at 30–1500 MHz can fulfill the requirement of high-shielding materials. Such properties are attributed to the regular arrangement of Mg_2Sn precipitates in the alloys. Compared with other shielding Mg-based alloys or composites, Mg-xSn-Zn-Ca-Ce alloys have higher strength. In particular, the 3Sn alloy achieves a UTS of 339 MPa owing to grain refinement, texture strengthening and precipitation strengthening, as shown in Figs. 9(a)–(c).

At present the shielding properties of Mg-based composite materials in which the primary shielding mechanisms are SE_R and SE_B have recently become a research hotspot. The SE of shielding Mg-based composites is remarkably improved at high frequencies. A desirable shielding Mg-9Li matrix composite containing $Ni_{0.4}Zn_{0.4}Co_{0.2}Fe_2O_4$ fabricated by multi-layer composite rolling has been developed [130]. Fig. 10(a) shows the schematic structure of this Mg-9Li/NZCF composite. NZCF particles are evenly distributed throughout the multi-layer Mg-9Li matrix. Mg-9Li alloy serves as the reflecting layer, and NZCF particles serve as the multiple reflection layer. The shielding capability can be regulated and controlled by adding nano-scale Ni-Zn-Co ferrites, which increases the NZCF content of the alloy, as indicated in Figs. 10(c) and (d). The total SE of the alloy reaches 99 dB at a high frequency of 12 GHz. A novel Mg-Li-Zn-Gd/MWCNTs composite with high EMI SE and strength

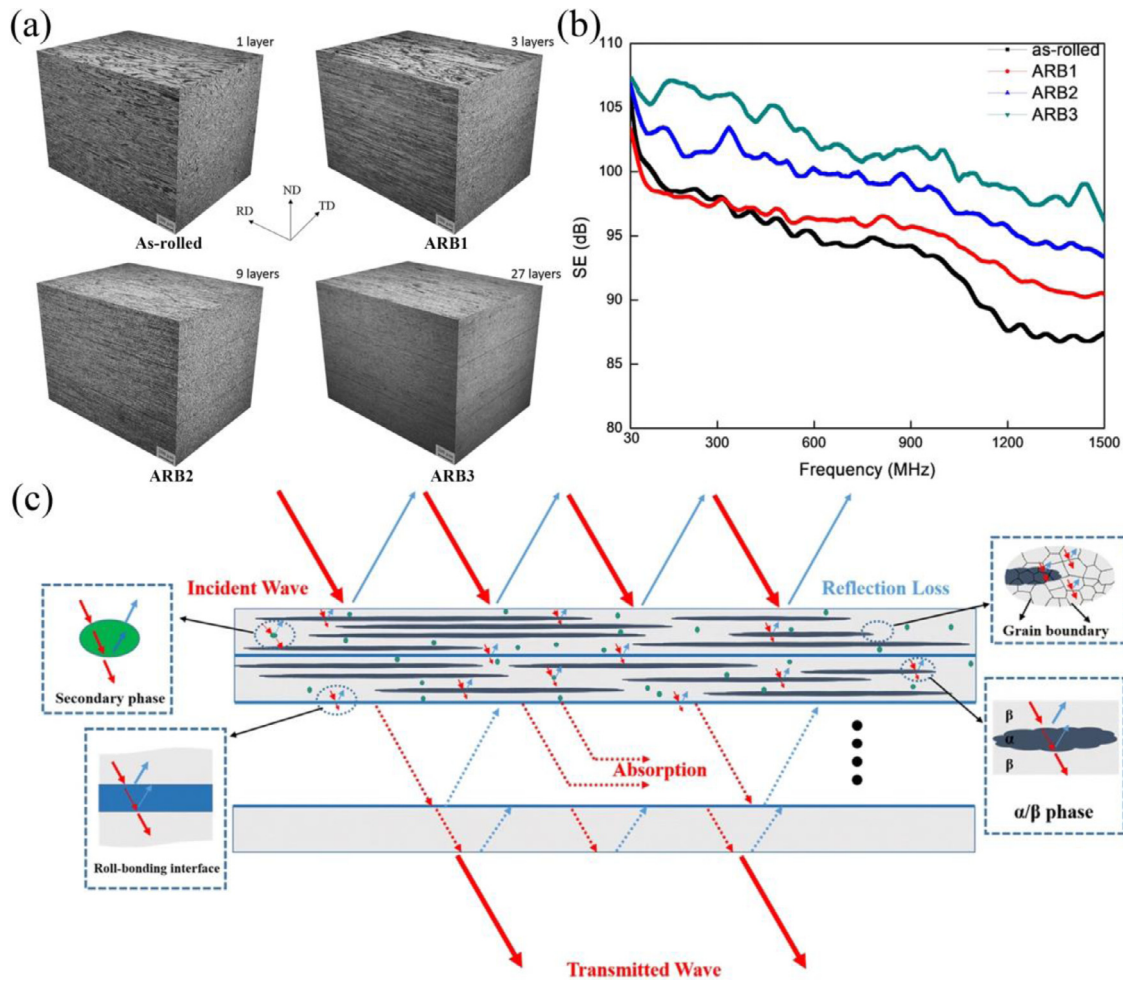


Fig. 8. (a) Three-dimensional optical micrographs of each pass, (b) SE curves, and (c) multilayer interface electromagnetic shielding mechanism of duplex-phase Mg–9Li–3Al–1 Zn alloy processed by ARB, respectively [132].

Table 5
Electrical conductivity, SE and mechanical properties of other shielding Mg alloys.

Materials	Processing conditions	SE/dB	SE/dB	Mechanical properties.			Ref
		($f = 800$ MHz)	($f = 1200$ MHz)	UTS (MPa)	YS (MPa)	EL (%)	
Mg–9Li–3Al–1Zn	As-rolled	95	88	194	152	24.1	[132]
	Accumulative roll bonding by one pass	96	92	215	188	23	[132]
	Accumulative roll bonding by two passes	99	96	~220	~190	~20	[132]
	Accumulative roll bonding by three passes	101	99	241	208	14.5	[132]
Mg–9Li	As-cast	91	86	124	87	34.1	[25]
	20% hot rolled	96	91	142	133	25.8	[25]
	50% hot rolled	98	95	166	154	19.1	[25]
	80% hot rolled	102	96	171	161	17.6	[25]
	First pass accumulative roll bonding	~68	~66	–	–	–	[26]
	Second pass accumulative roll bonding	~74	~68	–	–	–	[26]
	Third pass accumulative roll bonding	~74	~71	–	–	–	[26]
Mg–3Sn–1Zn–0.2Ca–0.3Ce	Fourth pass accumulative roll bonding	~77	~74	–	–	–	[26]
	As-cast	98	90	241	100	5.6	[134]
Mg–3Sn–2Zn–0.2Ca–0.3Ce	Hot rolled + T4 (480 °C, 24 h) + T5 (180 °C, 35 h)	88	81	334	228	4.8	[134]
	As-cast	95	83	290	71	8.2	[134]
Mg–3Sn–3Zn–0.2Ca–0.3Ce	Hot rolled + T4 (480 °C, 24 h) + T5 (180 °C, 35 h)	90	85	355	222	9.9	[134]
	As-cast	95	80	326	135	4.9	[134]
	Hot rolled + T4 (480 °C, 24 h) + T5 (180 °C, 35 h)	89	85	371	228	7.7	[134]

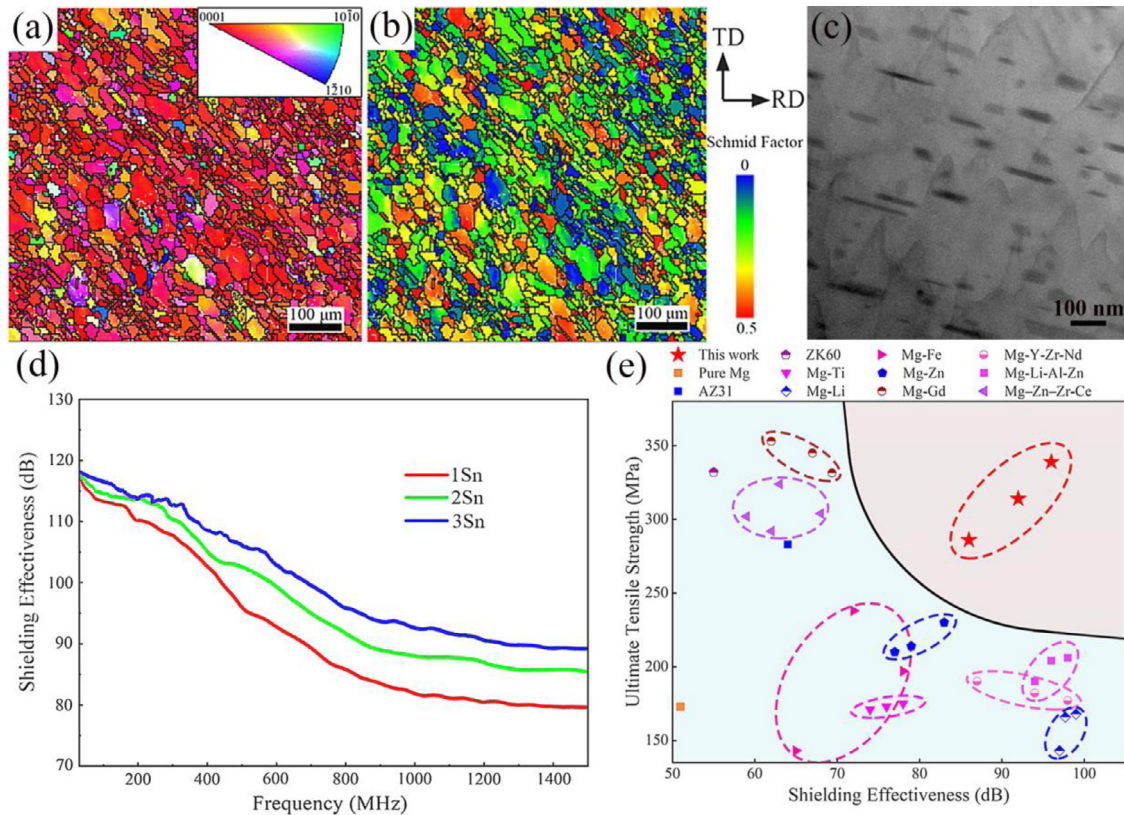


Fig. 9. (a) IPF maps, (b) distribution of SFs for basal slip, and (c) bright-field TEM images in aged Mg-3Sn-Zn-Ca-Ce alloys. (d) SE curves of Mg-xSn-Zn-Ca-Ce alloys. (e) SE at the frequency of 800 MHz and UTS of aged Mg-xSn-Zn-Ca-Ce alloys and other Mg-based materials [134].

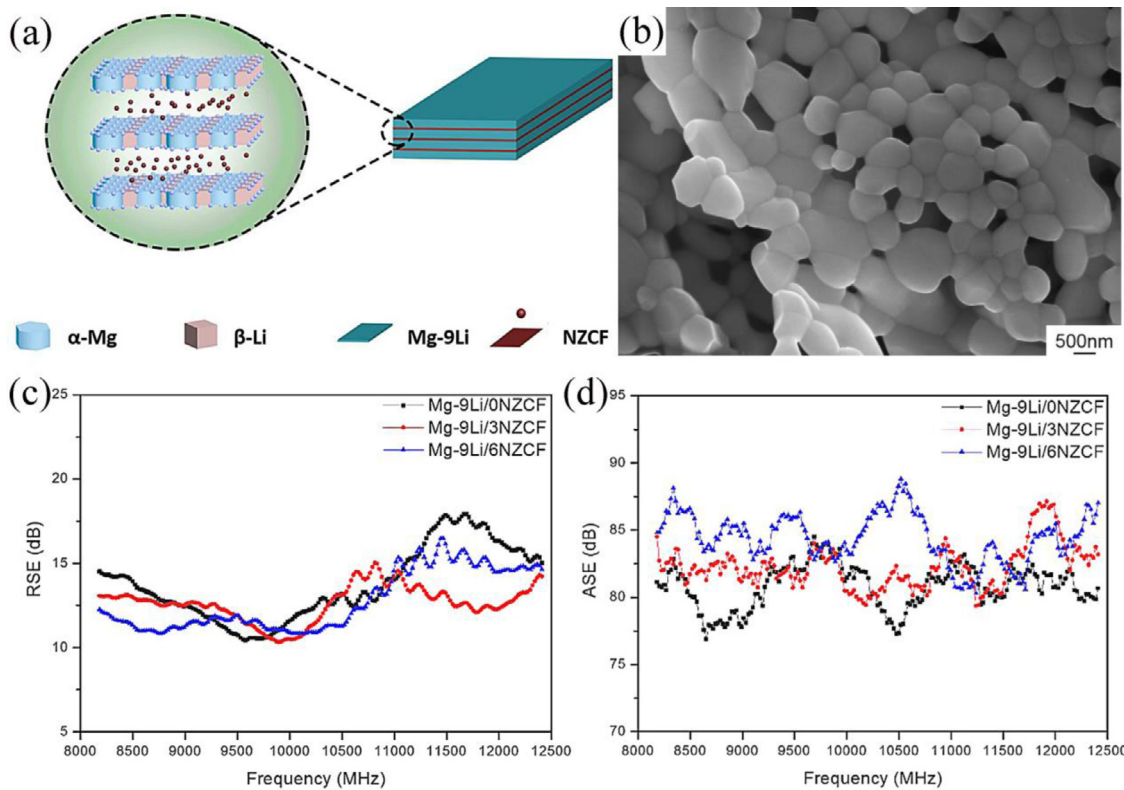


Fig. 10. (a) Schematic structure of Mg-9Li/NZCF composite. (b) SEM image of NZCF particles. (c) and (d) are the SE curves of Mg-9Li/xNZCF ($x = 0, 3, 6$ wt%) composites, respectively [135].

Table 6

Summary for total EMI SE of selected other new Mg alloys at high frequency.

Materials	SE/dB ($f = 9$ GHz)	SE/dB ($f = 12$ GHz)	Ref.
Mg–9Li matrix composite containing 3 wt.% Ni _{0.4} Zn _{0.4} Co _{0.2} Fe ₂ O ₄ (NZCF)	~96	~99	[130]
Mg/15 wt.% Fe (Mg iron micro-composites)	~76	~74	[27]
Mg/5 wt% Ti micro-composites	~75	~69	[30]
Mg–9Li–3Zn–0.5Gd/MWCNTs by C-ARB5	~91	~96	[135]

(X-band) was fabricated, and the EMI SE of the ARB5 (five accumulative roll bonding cycles) sheet in the X-band frequency range was found to be 77–96 dB [135]. MWCNTs are uniformly distributed in the Mg–Li matrix after ARB5. Improvement in the shielding properties of this composite is mainly attributed to the ability of the uniformly distributed MWCNTs to induce the precipitation of ultra-fine nano-scale W-phase. Additionally, other high EMI shielding Mg-based composite materials, such as a Mg–iron micro-composite [27] and pure Mg added with diamagnetic Ti micro-particulates [30], were also reported. The SE values of these Mg-based materials are listed in Table 6.

6. Remarks

The shielding Mg alloys as functional materials are becoming an emerging focus and anticipated to develop significantly in new Mg materials. Numerous studies on shielding Mg alloys have been carried out in recent years. This paper systematically summarizes the factors affecting the shielding properties of Mg alloys, including grain size, texture, alloying elements and second phase. Recent progress on EMI shielding Mg alloys, such as Mg–Zn, Mg–Al, Mg–Mn, Mg–RE and other new materials, is also reviewed.

Some remarkable results on the EMI SE of Mg alloys have been achieved by controlling the factors influencing the shielding properties of these alloys. The development of RE-free or low-RE Mg alloys with superior shielding properties and high mechanical properties simultaneously is more prominent, such as Mg–Zn–Y–Ce–Zr and Mg–Sn–Zn–Ca–Ce alloys. The extruded Mg–5Zn–1Ce–2Y–0.5Zr alloy exhibits an SE of 79–118 dB over the whole frequency range tested and a yield strength of over 400 MPa under different state. The superior shielding properties of Mg–3Sn–Zn–Ca–Ce alloy, with an SE of 91–114 dB, can fulfill the requirements of high-shielding materials. Additionally, the shielding Mg-based composite materials are closely concerned because of their specific structure that effectively reflect and multiple reflect electromagnetic waves.

Although the research and development of shielding Mg alloys has been carefully conducted, more work needs to be done in this area. The effect of grain size (at the nanoscale) on the SE of Mg alloys remains unknown. Controlling the grain size, texture, second phase and defects reasonably and simultaneously through heat treatment, deformation and alloying or micro-alloying is essential to obtain materials with good properties. The optimal parameters for developing Mg alloys with super-shielding properties must also be

determined. Additionally, the relatively low strength of Mg alloys is a problem that must be addressed, and the simultaneous improvement of EMI SE and mechanical properties is vital. While developing Mg alloys with high SE, other functional properties such as damping and thermal conductivity also need to be investigated systematically to develop multi-functional materials.

Acknowledgments

The authors would like to thank the financial supports from the National Natural Science Foundation of China (52171103), Fundamental Research Funds for the Central Universities (2020CDJDPT001 and cqu2018CDHB1A08), Guangdong Major Project of Basic and Applied Basic Research (2020B0301030006), Natural Science Foundation of Chongqing, China (cstc2019jcyj-msxmX0505), Science and Technology Research Program of Chongqing Municipal Education Commission (KJQN202101234) and Opened-end Foundation of Chongqing Light Alloy Materials and Processing Engineering Technology Research Center (GCZX201902).

References

- J. Thomassin, C. Jérôme, T. Pardoën, C. Bailly, I. Huynen, C. Detrembleur, Mater. Sci. Eng. R Rep. 74 (2013) 211–232.
- C. Liu, L. Wang, S. Liu, L. Tong, X. Liu, Adv. Indus. Eng. Polymer Res. 3 (2020) 149–159.
- Z. Luo, X. Chen, K. Song, C. Liu, Y. Dai, D. Zhao, F. Pan, Acta Metall. Sin.-Engl. 32 (2019) 817–824.
- D.D.L. Chung, Mater. Chem. Phys. 255 (2020) 123587.
- A.K. Singh, A. Shishkin, T. Koppel, N. Gupta, Compos. B. Eng. 149 (2018) 188–197.
- H.D. Shetty, A. Patra, V. Prasad, J. Magn. Magn. Mater. 525 (2021) 167678.
- D.D.L. Chung, Carbon N Y 39 (2001) 279–285.
- J. Zhang, Z. Wang, J. Li, Y. Dong, A. He, G. Tan, Q. Man, B. Shen, J. Wang, W. Xia, J. Shen, X. Wang, J. Mater. Sci. Technol. 96 (2022) 11–20.
- N.J. AbuAlRoos, N.A.Baharul Amin, R. Zainon, Radiat. Phys. Chem. 165 (2019) 108439.
- K.S. Sista, S. Dwarapudi, D. Kumar, G.R. Sinha, A.P. Moon, J. Alloy. Compd. 853 (2021) 157251.
- S. Xie, Z. Ji, L. Zhu, J. Zhang, Y. Cao, J. Chen, R. Liu, J. Wang, J. Build. Eng. 27 (2020) 100963.
- Z. Shen, J. Chen, B. Li, G. Li, Z. Zhang, X. Hou, J. Alloy. Compd. 815 (2020) 152388.
- K. Qian, Q. Li, A. Sokolov, C. Yu, P. Kulik, O. Fitchorova, Y. Chen, C. Chinnasamy, V.G. Harris, J. Mater. Sci. Technol. 83 (2021) 256–263.
- H. Oh, R. Umapathi, O. Omelianovich, V. Dao, J. Jeong, G. Lee, H. Choi, Thin Solid Films 676 (2019) 75–86.

- [15] G. Park, S. Kim, G. Park, N. Lee, J. Build. Eng. 35 (2021) 101982.
- [16] I. Yu, J. Ko, T. Kim, D.S. Lee, N.D. Kim, S. Bae, S. Lee, J. Choi, S.S. Lee, Y. Joo, Carbon N Y 167 (2020) 523–529.
- [17] M. Wang, X. Tang, J. Cai, H. Wu, J. Shen, S. Guo, Carbon N Y 177 (2021) 377–402.
- [18] S. You, Y. Huang, K.U. Kainer, N. Hort, J. Magnes. Alloy. 5 (2017) 239–253.
- [19] H. Pan, Y. Ren, H. Fu, H. Zhao, L. Wang, X. Meng, G. Qin, J. Alloy. Compd. 663 (2016) 321–331.
- [20] B. Wu, J. Li, J. Ye, J. Tan, L. Liu, J. Song, X. Chen, F. Pan, Vacuum 183 (2021) 109833.
- [21] Y. Yang, X. Xiong, J. Chen, X. Peng, D. Chen, F. Pan, J. Magnes. Alloy. 9 (2021) 705–747.
- [22] C. Liu, X. Chen, Y. Yuan, W. Zhang, Y. Zhang, F. Pan, J. Mater. Sci. Technol. 78 (2021) 20–29.
- [23] L. Liu, F. Pan, X. Chen, Y. Huang, B. Song, H. Yang, N. Hort, Vacuum 155 (2018) 445–455.
- [24] L. Liu, X. Chen, J. Wang, L. Qiao, S. Gao, K. Song, C. Zhao, X. Liu, D. Zhao, F. Pan, J. Mater. Sci. Technol. 35 (2019) 1074–1080.
- [25] J. Wang, R. Wu, J. Feng, J. Zhang, L. Hou, M. Zhang, Mater. Charact. 157 (2019) 109924.
- [26] J. Hou, Q.L. Zhang, Y.X. Niu, F.K. Ning, Q.C. Le, Mater. Res. Express 5 (2018) 66533.
- [27] R. Pandey, S. Tekumalla, M. Gupta, Compos. B. Eng. 163 (2019) 150–157.
- [28] K. Song, F.S. Pan, X.H. Chen, Z.H. Zhang, A.T. Tang, J. She, Z.W. Yu, H.C. Pan, X.Y. Xu, Mater. Lett. 157 (2015) 73–76.
- [29] K. Song, F. Pan, X. Chen, A. Tang, H. Pan, S. Luo, Mater. Res. Innov. 18 (2014) S4–S193.
- [30] R. Pandey, S. Tekumalla, M. Gupta, J. Alloy. Compd. 770 (2019) 473–482.
- [31] L. Liu, X. Chen, F. Pan, S. Gao, C. Zhao, J. Alloy. Compd. 688 (2016) 537–541.
- [32] J. Song, J. She, D. Chen, F. Pan, J. Magnes. Alloy. 8 (2020) 1–41.
- [33] M. Rakshith, P. Seenuvasaperumal, J. Magnes. Alloy. 9 (2021) 1692–1714.
- [34] C. Liu, X. Chen, J. Chen, A. Atrens, F. Pan, J. Magnes. Alloy. 9 (2021) 1084–1097.
- [35] J. Xie, J. Zhang, Z. You, S. Liu, K. Guan, R. Wu, J. Wang, J. Feng, J. Magnes. Alloy. 9 (2021) 41–56.
- [36] A. Gungor, A. Incesu, J. Magnes. Alloy. 9 (2021) 241–253.
- [37] C. Zhao, Z. Li, J. Shi, X. Chen, T. Tu, Z. Luo, R. Cheng, A. Atrens, F. Pan, J. Magnes. Alloy. 7 (2019) 672–680.
- [38] S. Ouyang, G. Yang, H. Qin, C. Wang, S. Luo, W. Jie, J. Magnes. Alloy (2021), doi:10.1016/j.jma.2021.06.016.
- [39] I.V. Antonets, Y.A. Golubev, V.I. Shcheglov, S. Sun, Curr. Appl. Phys. 29 (2021) 97–106.
- [40] X. Li, Z. Tao, B. Hao, Q. Kong, Z. Liu, Z. Liu, Q. Guo, L. Liu, Scripta Mater 187 (2020) 407–412.
- [41] Y. Chen, J. Li, T. Li, L. Zhang, F. Meng, Carbon N Y 180 (2021) 163–184.
- [42] S. Liu, S. Qin, Y. Jiang, P. Song, H. Wang, Compos. Part A Appl. Sci. Manuf. 145 (2021) 106376.
- [43] R.L.H.P.J.F. Garrett, Nav. Eng. J. (1982).
- [44] S. Geetha, K. Kumar, C. Rao, M. Vijayan, D.C. Trivedi, J. Appl. Polym. Sci. 112 (2010) 2073–2086.
- [45] D.D.L. Chung, Mater. Chem. Phys. 255 (2020) 123587.
- [46] J. Chen, Z. Zhu, H. Zhang, S. Tian, S. Fu, Mater. Design 204 (2021) 109695.
- [47] S. Gupta, N. Tai, Carbon N Y 152 (2019) 159–187.
- [48] C. Wang, V. Murugadoss, J. Kong, Z. He, X. Mai, Q. Shao, Y. Chen, L. Guo, C. Liu, S. Angaiah, Z. Guo, Carbon N Y 140 (2018) 696–733.
- [49] N. Maruthi, M. Faisal, N. Raghavendra, Synthetic Met. 272 (2021) 116664.
- [50] J. Thomassin, C. Jérôme, T. Pardoën, C. Bailly, I. Huynen, C. Detrembleur, Mater. Sci. Eng. R Rep. 74 (2013) 211–232.
- [51] S. Rahimpour, M. Kiyani, S.E. Hodges, D.A. Turner, Clin. Neurol. Neurosurg. 203 (2021) 106577.
- [52] S. Xie, Z. Ji, L. Zhu, J. Zhang, Y. Cao, J. Chen, R. Liu, J. Wang, J. Build. Eng. 27 (2020) 100963.
- [53] I. Yu, J. Ko, T. Kim, D.S. Lee, N.D. Kim, S. Bae, S. Lee, J. Choi, S.S. Lee, Y. Joo, Carbon N Y 167 (2020) 523–529.
- [54] S. Guo, H. Xu, M. Dong, M. Peng, C. Liu, C. Shen, Appl. Surf. Sci. 525 (2020) 146569.
- [55] A. Kausar, in: Chapter 9 - Electromagnetic interference Shielding Effectiveness of Polymer nanocomposites, Conducting Polymer-Based Nanocomposites, A. Kausar, Elsevier, 2021, pp. 211–236.
- [56] X. Chen, J. Liu, Z. Zhang, F. Pan, Mater. Design 42 (2012) 327–333.
- [57] K. Chandra Babu Naidu, S. RoopasKiran, W. Madhuri, Mater. Res. Bull. 89 (2017) 125–138.
- [58] D. Kumar, A. Moharana, A. Kumar, Mater. Today Chem. 17 (2020) 100346.
- [59] Y. Li, M. Zha, H. Jia, S. Wang, H. Zhang, X. Ma, T. Tian, P. Ma, H. Wang, J. Magnes. Alloy. 9 (2021) 1556–1566.
- [60] H. Liao, M. Zhan, C. Li, Z. Ma, J. Du, J. Magnes. Alloy. 9 (2021) 1211–1219.
- [61] Q. Zeng, Y. Zhang, K. Li, Y. Zhuang, J. Li, Y.J. Yuan, D. Yin, J. Magnes. Alloy (2021), doi:10.1016/j.jma.2021.05.022.
- [62] W. Xu, J. Yu, L. Jia, C. Gao, Z. Miao, G. Wu, G. Li, Z. Zhang, J. Magnes. Alloy. (2021), doi:10.1016/j.jma.2021.03.021.
- [63] H. Chen, J. Wang, X. Meng, Y. Xie, Y. Li, L. Wan, Y. Huang, Mater. Lett. 303 (2021) 130524.
- [64] K. Song, Study On Electromagnetic Shielding Properties of Magnesium Alloys, Chongqing University, 2015.
- [65] R. Pandey, S. Tekumalla, M. Gupta, J. Mater. Sci-Mater. El. 29 (2018) 9728–9739.
- [66] R. Pal, S. Lata Goyal, I.Rawal Asha, Mater. Sci. Eng. B-Adv. 270 (2021) 115227.
- [67] X.H. Chen, L. Lu, K. Lu, J. Appl. Phys. 102 (2007) 83708.
- [68] Y. Li, P. Hou, Z. Wu, Z. Feng, Y. Ren, H. Choo, Mater. Design 202 (2021) 109562.
- [69] M.J. Hao, W.L. Cheng, L.F. Wang, E. Mostaed, L.P. Bian, H.X. Wang, X.F. Niu, J. Magnes. Alloy. 8 (2020) 899–909.
- [70] C. Wang, H. Ning, S. Liu, J. You, T. Wang, H. Jia, M. Zha, H. Wang, Scripta Mater 204 (2021) 114119.
- [71] S.K. Woo, R. Pei, T. Al-Samman, D. Letzig, S. Yi, J. Magnes. Alloy. (2021), doi:10.1016/j.jma.2021.07.003.
- [72] L.M. Yao, Effects of Electromagnetic Shielding Effectiveness on Microstructure and Texture of Magnesium Alloy, Shenyang Ligong University, 2009.
- [73] T. Chen, Q. Gao, Y. Yuan, T. Li, Q. Xi, T. Liu, A. Tang, A. Watson, F. Pan, J. Magnes. Alloy. (2021), doi:10.1016/j.jma.2021.06.014.
- [74] X. Du, F. Wang, Z. Wang, L. Zhou, Z. Liu, P. Mao, J. Magnes. Alloy. (2021), doi:10.1016/j.jma.2021.05.015.
- [75] H. Pan, F. Pan, J. Peng, J. Gou, A. Tang, L. Wu, H. Dong, J. Alloy. Compd. 578 (2013) 493–500.
- [76] V.E. Bazhenov, A.V. Koltygin, M.C. Sung, S.H. Park, Y.V. Tselovalnik, A.A. Stepashkin, A.A. Rizhsky, M.V. Belov, V.D. Belov, K.V. Matyutin, J. Magnes. Alloy. 9 (2021) 1567–1577.
- [77] X.L. Cui, X.H. Li, H. Ye, H.W. Cui, H. Li, Y.K. Pan, R. Feng, Y.Y. Wu, X.F. Liu, J. Alloy. Compd. 885 (2021) 160959.
- [78] S. Li, X. Yang, J. Hou, W. Du, J. Magnes. Alloy. 8 (2020) 78–90.
- [79] D. Munalli, G. Dimitrakis, D. Chronopoulos, S. Greedy, A. Long, Compos. B. Eng. 173 (2019) 106906.
- [80] S. Das, S. Sharma, T. Yokozeki, S. Dhakate, Compos. Struct. 261 (2021) 113293.
- [81] R. Kumar, S. Sahoo, E. Joanni, R.K. Singh, W.K. Tan, K.K. Kar, A. Matsuda, Carbon N Y 177 (2021) 304–331.
- [82] X. Lei, X. Zhang, A. Song, S. Gong, Y. Wang, L. Luo, T. Li, Z. Zhu, Z. Li, Compos. Part A Appl. Sci. Manuf. 130 (2020) 105762.
- [83] H. Wang, K. Teng, C. Chen, X. Li, Z. Xu, L. Chen, H. Fu, L. Kuang, M. Ma, L. Zhao, Mater. Lett. 186 (2017) 78–81.

- [84] S.A. Mathews, D.R. Babu, *Curr. Appl. Phys.* 29 (2021) 39–53.
- [85] C. Yang, F. Pan, X. Chen, N. Luo, *Appl. Phys. A* 123 (2017) 1–7.
- [86] X. Xu, X. Chen, W. Du, Y. Geng, F. Pan, *J. Mater. Sci. Technol.* 33 (2017) 926–934.
- [87] H. Abbasi, M. Antunes, J.I. Velasco, *Prog. Mater. Sci.* 103 (2019) 319–373.
- [88] X. Chen, J. Liu, F. Pan, *J. Phys. Chem. Solids* 74 (2013) 872–878.
- [89] X. Chen, L. Liu, J. Liu, F. Pan, *Mater. Design* 65 (2015) 360–369 (1980–2015).
- [90] X. Chen, L. Liu, F. Pan, J. Mao, X. Xu, T. Yan, *Mater. Sci. Eng. B-Adv.* 197 (2015) 67–74.
- [91] C. Xianhua, G. Yuxiao, P. Fusheng, *Rare Metal Mat. Eng.* 45 (2016) 13–17.
- [92] G. Zhang, S. Qin, L. Yan, X. Zhang, *Mater. Charact.* 174 (2021) 111042.
- [93] S. Gao, X. Chen, F. Pan, K. Song, C. Zhao, L. Liu, X. Liu, D. Zhao, *Sci. Rep.* 8 (2018) 1625.
- [94] Z.C. Xu, *The Study On Microstructure and Electromagnetic Shielding Properties of Mg-Zn-Y Alloys*, Kunming University of Science and Technology, 2018.
- [95] S. Li, X. Yang, J. Hou, W. Du, *J. Magnes. Alloy.* 8 (2020) 78–90.
- [96] N. Balasubramani, G. Wang, M.A. Easton, D.H. StJohn, M.S. Dargusch, *J. Magnes. Alloy.* 9 (2021) 829–839.
- [97] Z. Gui, F. Wang, J. Zhang, D. Chen, Z. Kang, *J. Magnes. Alloy.* (2021), doi:10.1016/j.jma.2021.03.023.
- [98] W. Guo, W. Bian, H. Xue, X. Zhang, *J. Magnes. Alloy.* (2021), doi:10.1016/j.jma.2020.12.011.
- [99] X. Chen, L. Liu, F. Pan, L. Qiao, *Mater. Res. Innov.* 18 (2014) S4–S187.
- [100] J. Li, H. Ding, B. Li, L. Wang, *Mater. Sci. Eng. A* 819 (2021) 141464.
- [101] M. Goto, T. Yamamoto, S.Z. Han, T. Utsunomiya, S. Kim, J. Kitamura, J.H. Ahn, S.H. Lim, J. Lee, *Mater. Lett.* 288 (2021) 129353.
- [102] X. Lin, Y. Kuo, L. Wang, J. Ye, C. Zhang, L. Wang, K. Guo, *T. Nonferrous. Metal. Soc.* 31 (2021) 1587–1598.
- [103] M. Lotfpour, C. Dehghanian, M. Emamy, A. Bahmani, M. Malekan, A. Saadati, M. Taghizadeh, M. Shokouhimehr, *J. Magnes. Alloy.* (2021), doi:10.1016/j.jma.2021.01.002.
- [104] M.G. Jiang, C. Xu, H. Yan, T. Nakata, Z.W. Chen, C.S. Lao, R.S. Chen, S. Kamado, E.H. Han, *J. Magnes. Alloy.* 9 (2021) 1797–1805.
- [105] J. Luo, H. Yan, L.W. Lu, R.S. Chen, A.R. Wu, F.C. Yin, *J. Alloy. Compd.* 883 (2021) 160813.
- [106] L. Liu, X. Chen, F. Pan, A. Tang, X. Wang, J. Liu, S. Gao, *Mater. Sci. Eng. A* 669 (2016) 259–268.
- [107] L. Liu, X. Chen, H. Wang, F. Pan, J. Wang, *J. Mater. Eng. Perform.* 27 (2018) 4722–4731.
- [108] L.Z. Liu, *Study On Electromagnetic Shielding and Mechanical Properties of Mg-Zn-Y-Ce-Zr magnesium Alloys*, Chongqing University, 2018.
- [109] R. Shi, *J. Magnes. Alloy.* (2021), doi:10.1016/j.jma.2021.02.007.
- [110] J. Kang, J. Park, K. Song, C. Oh, O. Shchyglo, I. Steinbach, *J. Magnes. Alloy.* (2021), doi:10.1016/j.jma.2021.04.014.
- [111] M. Mezbahul-Islam, A.O. Mostafa, M. Medraj, A. Singh, *J Mater* 2014 (2014) 704283.
- [112] J. Wang, L. Niu, Y. Zhang, J. Chen, J. Jiang, D. Song, B. Li, G. Ying, J. Cheng, A. Ma, *J. Magnes. Alloy.* (2021), doi:10.1016/j.jma.2021.06.006.
- [113] J. Miao, W. Sun, A.D. Klärner, A.A. Luo, *Scripta Mater.* 154 (2018) 192–196.
- [114] J. Wei, Q. Wang, L. Zhang, D. Yin, B. Ye, H. Jiang, W. Ding, *Mater. Lett.* 246 (2019) 125–128.
- [115] Q. Yang, K. Guan, B. Li, F. Meng, S. Lv, Z. Yu, X. Zhang, J. Zhang, J. Meng, *J. Alloy. Compd.* 766 (2018) 902–907.
- [116] Z.H. Zhang, *Influence of Deformation and Heat Treatment on the Electromagnetic Shielding Property of AZ Magnesium Alloy*, Chongqing University, 2013.
- [117] Y.W. Shen, *Hot Working Technology* 47 (2018) 121–123, doi:10.14158/j.cnki.1001-3814.2018.12.031.
- [118] F. Gao, *Study On the Preparation and Organization of Mg-Al-Zn alloy Used For Electromagnetic Shielding Performance*, Xi'an Technological University, 2016.
- [119] S.L. Guo, *Effect of Rare Earth La on Corrosion and Electromagnetic Shielding Property of AZ31 Magnesium Alloy*, Inner Mongolia University of Science & Technology, 2016.
- [120] X.H. Li, H.Y. Yang, *Light Alloy Fabric. Technol.* 44 (2016) 44–48, doi:10.13979/j.1007-7235.2016.02.008.
- [121] Y.L. Wang, *Hot Working Technology* 44 (2015) 47–49, doi:10.14158/j.cnki.1001-3814.2015.17.013.
- [122] Y.N. Luo, H.L. Huang, *Hot Working Technol.* 44 (2015) 105–107, doi:10.14158/j.cnki.1001-3814.2015.07.029.
- [123] G. Wu, C. Wang, M. Sun, W. Ding, *J. Magnes. Alloy.* 9 (2021) 1–20.
- [124] W. Zhao, E. Guo, K. Zhang, X. Tian, C. Tan, *Scripta Mater.* 199 (2021) 113863.
- [125] X. Jin, W. Xu, D. Shan, B. Guo, B.C. Jin, *Mater. Design* 199 (2021) 109384.
- [126] W. Kang, L. Lu, L. Feng, F. Lu, C. Gan, X. Li, *J. Magnes. Alloy.* (2021), doi:10.1016/j.jma.2021.05.019.
- [127] X.F. Zhao, *Influence of Extrusion Deformation and T5-treatment on Electromagnetic Shielding Property of Rare Earth Magnesium Alloy*, North University of China, 2017.
- [128] Y. Le, *Influence of Hot Working Technology on Electromagnetic Shielding Performance of Rare Earth Magnesium Alloy*, North University of China, 2018.
- [129] R. Liu, *Influence of Elements and Rolling on the Electromagnetic Shielding Performance of Magnesium Alloy*, Harbin Institute of Technology, 2016.
- [130] J. Wang, Y. Li, R. Wu, L. Xu, Z. Zhang, J. Feng, J. Zhang, L. Hou, Y. Jiao, *J. Alloy. Compd.* 843 (2020) 156053.
- [131] R. Pandey, S. Tekumalla, M. Gupta, *J. Alloy. Compd.* 770 (2019) 473–482.
- [132] J. Wang, L. Xu, R. Wu, J. Feng, J. Zhang, L. Hou, M. Zhang, *Acta Metall. Sin-Engl.* 33 (2020) 490–499.
- [133] S.Y. Gao, *Effect of Secondary Phases On the Electromagnetic Shielding Effectiveness of Magnesium Alloy*, Chongqing University, 2018.
- [134] J. Ye, X. Chen, Z. Luo, J. Li, Y. Yuan, J. Tan, F. Pan, *Adv. Eng. Mater.* (2021) 2100166.
- [135] J. Wang, L. Xu, R. Wu, D. An, Z. Wei, J. Wang, J. Feng, J. Zhang, L. Hou, M. Liu, *J. Alloy. Compd.* 882 (2021) 160524.